https://doi.org/10.1142/9789811278952_0008

Chapter 8

Collimation of HL-LHC Beams

S. Redaelli[a], A. Bertarelli[b], R. Bruce[a], F. Carra[b], A. Lechner[c], A. Mereghetti[d] and A. Rossi[c]

[a]*CERN, BE Department, Genève 23, CH-1211, Switzerland*
[b]*CERN, EN Department, Genève 23, CH-1211, Switzerland*
[c]*CERN, SY Department, Genève 23, CH-1211, Switzerland*
[d]*Centro Nazionale di Adroterapia Oncologica (CNAO), Pavia, Italy*

High-performance collimation systems are essential for operating modern hadron accelerators with large beam intensities efficiently and safely. In particular, at the LHC the collimation system ensures a clean disposal of beam halos in the superconducting environment. The challenges of the HL-LHC study pose more demanding requests for beam collimation. In this chapter, the upgraded collimation system for HL-LHC is presented. Various collimation solutions were elaborated to address the HL-LHC requirements and challenges. These are reviewed in the following, identifying the main upgrade baseline and pointing out advanced collimation concepts under consideration for further enhancement of the collimation performance.

1. Introduction

Because of the high stored energy of about 700 MJ for each of the full HL-LHC beams and the small transverse beam sizes [1], the HL-LHC beams have the potential for creating significant damage from uncontrolled beam losses. Even a local beam loss of a tiny fraction of the full beam in a superconducting magnet could cause a quench, and larger beam losses could easily cause damage to accelerator components. A variety of processes can cause unavoidable beam losses during normal and abnormal beam operation. Therefore, all beam losses must be tightly controlled. For this purpose, a multistage

collimation system has been installed in the LHC [2,3] to safely dispose of beam losses. Unlike other high-energy colliders, where the main purpose of collimation is typically to reduce experimental backgrounds, the LHC and the HL-LHC require efficient beam collimation during all stages of operation from injection to top energy. The requirement to operate efficiently and safely with high-intensity hadron beams at small colliding beam sizes entails significant challenges, which drive the key design aspects of the collimation system at the HL-LHC [4].

In addition to cleaning the unavoidable beam halo to prevent quenches of superconducting magnets, the collimation system must fulfil other important roles [5]. The collimators are the closest elements to the circulating beam and they must provide passive protection to any aperture bottleneck, in particular the triplet magnets around the experiments, with sufficient margins [6,7]. They help concentrate the radiation dose and activation to confined areas and provide local protection of equipment to improve its lifetime. In addition, collimators also clean collision debris products, with dedicated active collimators on the outgoing beams of each high-luminosity experiment [8,9]. Furthermore, collimation plays a role in keeping under control machine- and halo-induced experimental background [10,11]. Collimation also provides a crucial role for passive machine protection in case of any failure, e.g. injection and dump kicker failures [12] (see also Chapter 19).

For these requirements, the LHC collimation system features an unprecedented complexity compared to previous particle accelerators. The LHC collimation system used in Run 1 (2010–2013) [13] and Run 2 (2015–2018) [14] consisted of up to 108 movable collimators and 10 fixed-aperture absorbers, and provided an excellent cleaning efficiency above 99.99% [3], i.e. less than 10^{-4} of the primary beam losses reached the superconducting magnets. The highest cold losses occur in the dispersion suppressors (DSs) around IR7. Nevertheless, the system must be upgraded to cope with the new HL-LHC challenges. The LHC collimation system was designed to safely withstand beam lifetime drops down to 0.2 h during 10 s at maximum beam current at 7 TeV, corresponding to peak losses of up to 500 kW [3]. This increases to 945 kW for HL-LHC if a simple scaling by the total stored beam energy is applied. The Pb ion beam upgrade, targeting more than 20 MJ stored beam energy at luminosities around 7×10^{27} cm^{-2} s^{-1} [15] is also very challenging for beam collimation. In addition, given the low electrical conductivity

of the present primary and secondary collimator materials and their vicinity to the beam, these collimators contribute significantly to the machine impedance, which will become much more critical for beam stability with the higher HL-LHC brightness. Finally, the higher peak luminosity goal of the HL-LHC, about 5 times larger than the initial LHC design, demands an upgrade of the collimation around the high-luminosity collision points, both in terms of magnet protection and physics debris disposal.

2. The HL-LHC Multi-Stage Collimation System

The backbone of the HL-LHC collimation system will remain as it is for the current LHC, the betatron (IR7) and momentum (IR3) multi-stage cleaning systems installed in two separated warm insertions [2]. A very efficient halo cleaning is achieved by precisely placing blocks of materials close to the circulating beams, while respecting a pre-defined multi-stage collimator hierarchy (illustrated schematically in Fig. 1). Primary (TCP) and secondary (TCS) collimators are placed closest to the beam. Active shower absorbers (TCLA) catch the showers produced by upstream stages. Tertiary collimators

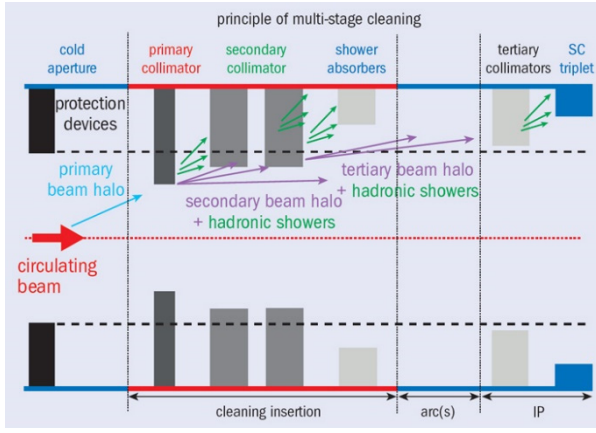

Fig. 1. Schematic illustration of the LHC multi-stage collimation cleaning system. Primary and secondary collimators (darkest grey) are closest to beam and are made of robust carbon-fibre-carbon composites. Shower absorbers and tertiary collimators (lighter grey) sit at larger apertures and are made of a tungsten alloy to improve absorption, in the shadow of protection devices (black). Collimators of different families are ordered in a pre-defined collimation hierarchy that must be respected to ensure the required system functionalities.

(TCTs) are located in front of the aperture bottlenecks in the final focusing system close to the experiments.

About 50% of the present LHC system will remain operational in HL-LHC, and the rest of the system will be replaced. Three main pillars of the HL-LHC collimation upgrade can be identified:

- Improved protection of the DS regions around IR7 and IR2 to mitigate local beam losses through new collimators (TCLD and TCPC). In IR2, one TCLD per side will be installed in the empty connection cryostat, to be used only for Pb ion operation; In IR7, one TCLD per side could be installed together with 11 T dipoles needed to make space for the collimator. However, the installation of the TCLDs in IR7 cannot take place before Long Shutdown 3 (LS3) and new primary crystal collimators TCPCs will be used in IR7 during ion operation in order to increase the cleaning efficiency and to lower the losses in the DS regions around IR7 (see Chapter 30).
- Reduction of the collimator-induced impedance to allow the operation of the larger-brightness beams of the HL-LHC: 9 out of 11 LHC secondary TCSG collimators will be replaced by a new low-impedance design (TCSPM).
- Improvement of the collimation of incoming and outgoing beams in the experimental insertions IR1 and IR5. Four tertiary collimators per beam and per high luminosity IR are needed to protect matching section and inner triplet from beam losses; three physics debris collimators and three fixed masks per beam and per high luminosity IR are needed to protect matching section and DS from collision debris.

In order to minimize the time spent outside physics operation, an improvement of the collimator setup time and the minimization of faults also requires a consolidation of the present system. The list of LHC (as of Run 2) and HL-LHC ring collimators are given in Table 1. Collimator types (with their collimation plane) and family names are introduced together with the number of units and their active material. The 2018 settings for β^*=25 cm and the HL-LHC baseline settings for β^*=15 cm are also listed. New collimators that are part of the HL-LHC upgrade will be installed in the DSs around IR2 and in IR7 ("DS cleaning" upgrade), in IR1/5 (IR upgrade) and IR7 (low-impedance upgrade). Approved consolidation activities include the replacement of four primary collimators with low-impedance ones made of molybdenum carbide-

Table 1. Collimators used in LHC and HL-LHC, including their abbreviated names, plane (H=horizontal, V=vertical, S=skew), the number of installed units, the material (CFC=carbon-fibre composite, W=heavy tungsten alloy (Inermet180), MoGr=molybdenum-graphite, CuCD= copper-diamond) and the operational openings in collision in units of beam σ. The LHC settings are given for p-p operating at β*=25 cm, as used in 2018, and the HL-LHC settings for β*= 15 cm. In both cases, a reference proton emittance of 2.5 μm has been used. The IR2 TCLD's and the crystal primary collimators are used only in ion operation.

Functional type	Name	Plane	Number		Material		Physics settings [σ]	
			LHC	HL	LHC	HL	LHC	HL
Primary IR3	TCP	H	2	2	CFC	CFC	17.7	17.7
Secondary IR3	TCS	H	8	8	CFC	CFC	21.3	21.3
Absorber IR3	TCLA	H, V	8	8	W	W	23.7	23.7
Passive absorber IR3	TCAP	--	4	4	W	W	--	--
Primary IR7	TCP	H, V, S	6	2	CFC	CFC	5.9	6.7
Primary crystal IR7	TCPC	H, V	--	4	Si	Si	--	6.5
Low-impedance primary IR7	TCP	H, V	--	4	--	MoGr	--	6.7
Secondary IR7	TCS	H, V, S	22	4	CFC	CFC	7.7	9.1
Low-impedance secondary IR7	TCS	H, V, S	--	18	--	MoGr	--	9.1
Absorber IR7	TCLA	H, V, S	10	10	W	W	11.8	12.7
Passive absorber IR7	TCAP	--	8	8	W	W	--	--
Passive absorber mask IR7	TCAPM	--	--	2	--	Steel	--	--
Dispersion suppressor IR7	TCLD	H	--	2	--	W	--	16.6
Dispersion suppressor IR2	TCLD	H	--	2	--	W	--	30
Tertiary IR2/IR8	TCT	H, V	8	8	W	W	17.7/ 43.8	17.7/ 43.8
Tertiary IR1/IR5	TCT	H	4	8	W	CuCD or W	9.2	10.4
Tertiary IR1/IR5	TCT	V	4	8	W	W	9.2	10.4
Physics debris IR1/IR5	TCL	H	12	12	Cu/W	W	18-41	14
Physics debris IR1/IR5 mask	TCLM	--	--	12	--	Cu and W	--	--
Dump protection IR6	TCDQ	H	2	2	CFC	CFC	8.6	10.1
	TCSP	H	2	2	CFC	CFC	8.6	10.1

graphite (MoGr) and of new passive absorber masks, planned for LS2. The other devices that are part of the present system will remain unchanged and operational for the HL-LHC era. Crystal primary collimators (TCPCs) for ion beam collimation, discussed in detail in Chapter 30, are also listed. Most collimators consist of two movable blocks, called 'jaws', placed symmetrically around the beam. The collimators are built as high-precision devices, with the key features of (i) a jaw flatness of about 40 μm; (ii) a surface roughness below 2 μm; (iii) a 5 μm positioning resolution (mechanical, controls); (iv) an overall setting reproducibility below 20 μm [16]; (v) a minimum gap below 0.5 mm; (vi) the capability to withstand heat loads of up to 6 kW in a steady-state regime (1 h beam lifetime) and of up to 30 kW in transient conditions (0.2 h beam lifetime) [17].

The initial LHC collimator design [18] has been improved by adding two beam position monitors (BPM pickups) on both extremities of each jaw [17,19-21]. This allows for fast collimator alignment as well as a continuous monitoring of the beam orbit with the possibility to interlock the beam position. After prototype tests in the SPS [22], several collimators with this design were installed and operated in LHC Run 2 [21]. All new HL-LHC collimators incorporate this feature that improves significantly the operational flexibility and β^* reach, contributing in particular to reaching β^*=25 cm in 2018 [7]. The improved flexibility in the IRs is particularly relevant for HL-LHC that will rely on complex levelling schemes, with frequent changes of orbit and optics. It is noted that the BPM feature cannot be integrated in the design of the crystal collimators that will thus be aligned with the standard BLM-based method.

3. Collimation Upgrade in the High-Luminosity Interaction Regions

The LHC Run 1 and Run 2 operation showed that protection of the IR superconducting magnets and experiments is a key asset for machine performance and efficient operation; the available aperture, to be protected in all operational phases, determines the transverse collimation hierarchy. With the pushed β^* and the increased beam intensity and luminosity of HL-LHC, protecting the machine aperture becomes even more challenging. In order to provide adequate protection, the HL-LHC collimation layout in IR1 and IR5 includes two pairs of TCTs (horizontal and vertical) on each *incoming beam*, as well as three physics debris absorbers (TCLs) and three fixed masks on each *outgoing*

beam. The layouts of Beam 1 and Beam 2 are symmetric, requiring a total of 20 movable collimators and 12 fixed masks. Fig. 2 shows the HL-LHC layout in IR1 together with the nominal LHC layout deployed in Run 1. The layout in IR5 is similar and contains the same upgrades.

The LHC tertiary collimators are located at positions that protect the triplet; in order to provide the necessary absorbance, they make use of a heavy tungsten alloy (Inermet 180). They effectively protect the downstream elements but are not robust against high beam losses, in particular during very fast beam failures that might occur if the beam dumping system does not trigger synchronously with the abort gap (an "asynchronous beam dump"). With the increase in bunch intensity of HL-LHC, this accident scenario becomes even more critical. Margins on collimator settings are added to the collimator hierarchy to minimize this risk [7]. In Run 2 a new optics with a specially matched phase advance between the extraction kickers and the TCTs was deployed, which was used to significantly push further the β^* performance of the LHC. A TCT design with improved robustness would provide an alternative way to reduce the hierarchy margins without introducing constraints on the optics. This gives more flexibility in the optics design, which is useful in particular for the HL optics baseline that features many other constraints.

The extensive experimental experience of beam impacts on collimator material samples at the CERN facility HiRadMat [23-26], where several new materials were studied, indicates that MoGr can improve the TCTP robustness by a factor of several hundreds, while copper-diamond (CuCD), featuring higher density (and hence better cleaning efficiency) and larger electrical conductivity, would still give about a factor 15 improvement in robustness [24]. Therefore, CuCD is the preferred material choice for the horizontal TCTs, although Inermet180, as used in the LHC TCTs, would not prevent reaching the HL-LHC baseline performance with the present optics baseline. The final decision will be taken in 2022 based on experience with a prototype collimator, which is being built with jaws in CuCD, and on the assessment of the final production costs for CuCD. The vertical tertiary collimators are still made of Inermet 180, since the critical losses from an asynchronous beam dump occur only in the horizontal plane.

In addition to improvements from increased robustness, the HL-LHC layout has additional aperture constraints [1] because the normalized aperture of the magnets up to Q5 is now smaller than in the present layout. Thus,

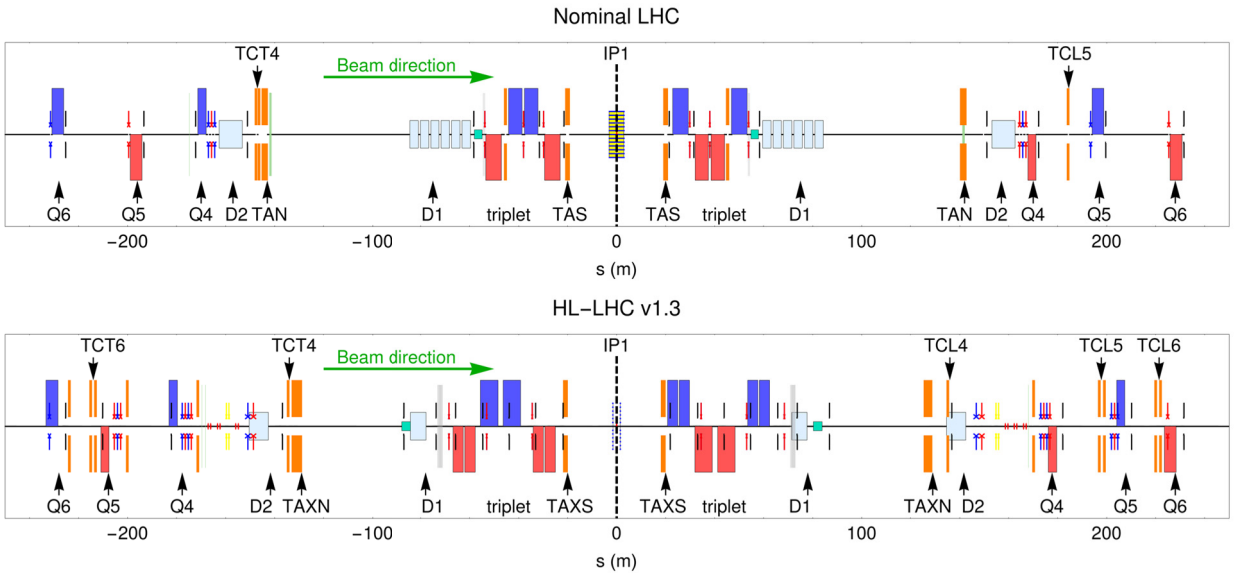

Fig. 2. The schematic layout in the experimental insertion IR1 for the nominal LHC as used in Run 1 (top) and HL-LHC v1.3 (bottom). Collimators are indicated in orange, quadrupoles in blue and red for the two polarities, and dipoles in light blue.

additional tertiary collimators are required in IR1/IR5 to protect the Q4 and Q5 quadrupole magnets. The present baseline includes a pair of new TCTP collimators in front of Q5, including one horizontal and one vertical, and another pair of TCTPs just upstream of the TAXN to protect the triplet, as for the nominal LHC.

The expected beam losses in the experimental insertions have been verified in simulations. Tracking simulations of the collimation mechanism using SixTrack [27,28] show that the proposed layout provides adequate protection of all magnets against cleaning losses [8]. Simulations of asynchronous beam dumps show that no direct losses are to be expected on the magnets, and losses of up to about 2×10^{10} protons could occur on the TCTs [12]. These losses consist of spread-out secondary protons, scattered out of upstream collimators, about a factor 5 below the onset of plastic deformation even for Inermet 180. This result relies on a matched fractional phase advance below 30° between the extraction kickers and the TCTs, as implemented in HL-LHC v1.3.

Further simulations of energy deposition during an asynchronous beam dump hitting a TCT show that there is no risk of damaging neither the experimental detectors nor the downstream magnets. Experimental background coming from the TCTs during normal operation is not expected to be problematic based on other recent studies [11].

The collimators on the outgoing beams, downstream of the high-luminosity experiments, must intercept both scattered primary beam particles and secondary particles generated by the collisions. The protection of the triplet from luminosity debris is discussed in Chapter 10, and here the focus is instead on the protection of the matching section. In Run 1, protection of the matching section was achieved by a single horizontal collimator in Cell 5, called TCL5. For Run 2, new TCLs were added in Cells 4 and 6, to cope with the higher luminosities and requirements from forward-physics experiments.

In HL-LHC, the ultimate levelled luminosity of 7.5×10^{34} $cm^{-2}s^{-1}$ will be about a factor three higher than the peak achieved at the beginning of the collision process during Run 2 in the LHC, which is a significant challenge for the collimation of physics debris. In addition, the absorber TAXN (the upgrade of the TAN, see Chapter 13) is less effective – because of the geometry of the reference trajectory and crossing angle, a significantly larger fraction of the scattered particles can pass through its opening than in the LHC (see also Chapter 15).

Therefore, several improvements are foreseen for the HL-LHC. The TCL4 needs to be upgraded to have thicker jaws [4] in order to intercept a larger fraction of the particles that have passed through the TAXN opening. This new collimator is called TCLX. In addition, fixed masks have to be installed on the IP side of Q4, Q5, and Q6. The TCL5 and TCL6 are also needed, and the material of all TCLs will be changed to a tungsten heavy alloy for better protection. Using this new layout, the highest power load in any magnet coil in the matching section stays below 1.5 mW/cm^3 at peak ultimate luminosity of 7.5×10^{34} cm^{-2}s^{-1}, which is far below the estimated quench limits. It should be noted also that the TCTs also play a role in protecting the outcoming-beam bore from the collision debris.

The design of the new IR collimators is challenging. Due to the larger β-functions in the HL-LHC high-luminosity insertions, the TCTs and TCLs in Cell 4 have to be opened to rather large gaps in mm to achieve the smaller normalized design openings in σ. To keep a maximum operational flexibility, a half gap of up to 40 mm could be needed, while it is limited to 30 mm in the present collimator design, so modifications are necessary. In addition, the transverse physical space available at this location in the HL-LHC tunnel is limited.

In order to provide the needed stroke and still fit in the horizontal space, a new two-in-one collimator design for the horizontal TCT and the TCL4 has been developed. A single vacuum tank houses the movable jaws acting on one beam and the vacuum chamber of the opposing, non-collimated, beam. A 3D model of this design is shown in Fig. 3. For the vertical TCT in Cell 4, a two-in-one design is not needed, however, a special design still has to be developed to implement the larger stroke of up to 40 mm.

4. Dispersion Suppressor Collimation Upgrades

The cleaning upgrades in the dispersion suppressor (DS) regions for HL-LHC is primarily driven by the increased risk of quenches from off-momentum losses. The DSs around IR7 are the main bottleneck in the LHC in terms of collimation leakage. A small fraction of protons interacting with the collimators in IR7 escape from the IR with a reduced magnetic rigidity. These protons, which are mainly single diffractive protons emerging from the TCPs, represent a source of local heat deposition in the cold DS magnets downstream

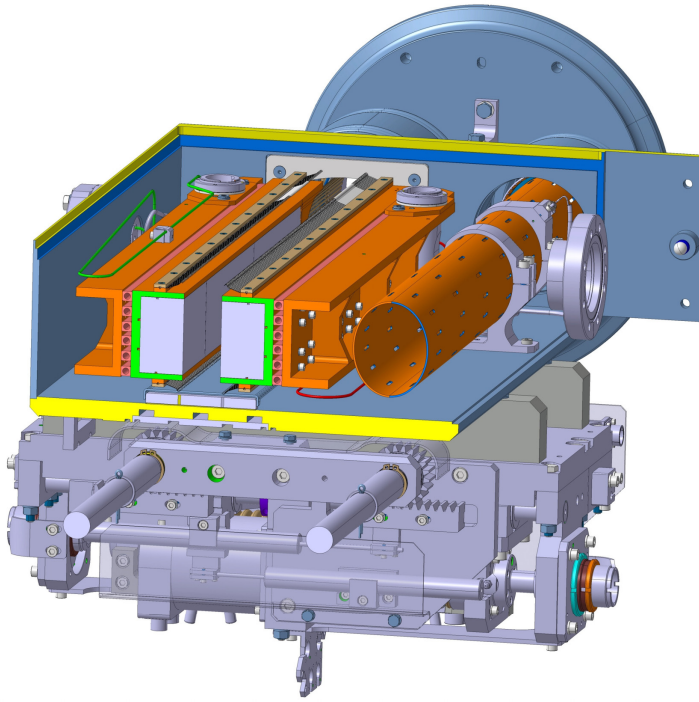

Fig. 3. Design of two-in-one collimators with a common vacuum tank housing both the movable jaws (left part) and the vacuum chamber of the opposing beam.

of IR7, where the dispersion starts to increase (see [29] and references therein). These losses are among the highest losses in cold magnets around the ring. In case of large drops in the beam lifetime, the impacted magnets risk quenching and the beams should be dumped by the BLMs before. This would result in costly downtime and reduced HL-LHC availability. The same mechanism inducing DS losses applies to secondary ion fragments produced in IR7 collimators during heavy ion operation. Although the intensities of heavy-ion beams are lower, they undergo numerous nuclear and electromagnetic interactions with the material of the primary collimators, creating an abundance of secondary ions with different mass and charge. Collimation of heavy-ion beams is therefore much less efficient than that of proton beams.

The design goal for the LHC, used also for HL-LHC, is that quenches and beam dumps should be avoided for a beam lifetime of 0.2 h for up to 10 s, or 1h beam lifetime for extended time periods [3]. This implies that the cleaning

system must sustain a higher power loss due to the higher beam intensity. Although such pessimistic lifetimes were rarely encountered in the LHC, this criterion is maintained in the HL-LHC design phase, where neither the quench limits at 7 TeV nor the operational performance are yet well known.

The acceptable losses in the DSs around IR7 were investigated with experimental quench tests with protons and Pb ions [30,31], and a quench was achieved in the heavy-ion test with a 6.37 Z TeV Pb beam [31,32]. A campaign of tracking studies using the SixTrack-FLUKA coupling [27] and energy deposition studies with FLUKA [33] managed to reproduce the experimental results within about a factor 3 [34,35]. This is considered a good agreement, given that the losses span many orders of magnitude and that there are large uncertainties and unknowns, in particular in terms of imperfections. Since the simulations underestimate the quench level inferred from beam experiments, all simulations for HL-LHC are scaled up by this factor.

Similar simulations have then been performed for HL-LHC for protons and Pb ions. If no upgrade is done, the peak power load in the superconducting coils in the DS, averaged over the cable width, is estimated at around 21 mW/cm^3 for protons and 57 mW/cm^3 for Pb ions during a beam lifetime drop to 0.2 h [4]. This should be compared with a quench limit of around 20 mW/cm^3, inferred from the quench tests and corresponding simulations. The proton losses are just above the limit and the Pb ion losses exceed it by almost a factor of 3. It is therefore clear that there is a need for a cleaning upgrade, at least for Pb ion beam operation.

To mitigate the risk of quenches, it is therefore foreseen to add local collimators, referred to as TCLDs, in the DSs, where the dispersion has already started rising. In IR7 this is only feasible with a major change of the cold layout. In order to make space for the new collimators, it is envisaged to replace, for each TCLD in IR7, an existing main dipole with two shorter 11 T dipoles. The 60 cm long TCLD, made of the tungsten alloy Inermet 180, will be located in the middle between the two 11 T magnets, as shown in Fig. 4. A photograph of the TCLD collimator is given in Fig. 5: as received at CERN and as installed in the IR2 DS (Feb. 2020). The TCLD will be integrated in a specially designed assembly, containing a beam pipe for the other beam, as well as a cryo-bypass. The system design is particularly complex due to the very limited space imposed by the surrounding cryogenic equipment. Therefore, the active length of the material had to be reduced to only 60 cm.

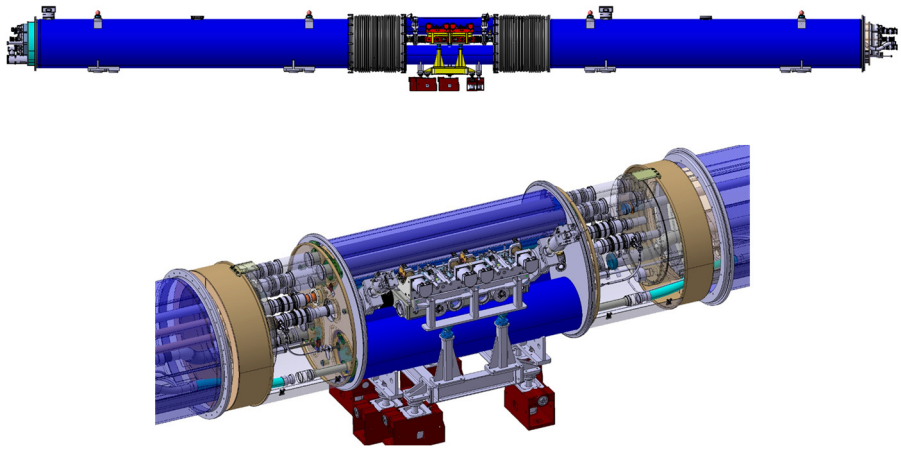

Fig. 4. Top: Schematic view of the assembly of two shorter 11 T dipoles with a collimator in between, which can replace one standard main dipole. Bottom: 3D model of a TCLD assembly showing the collimator (in grey, at the centre), the two short dipole cryostats and the connection cryostat. (Courtesy of L. Gentini).

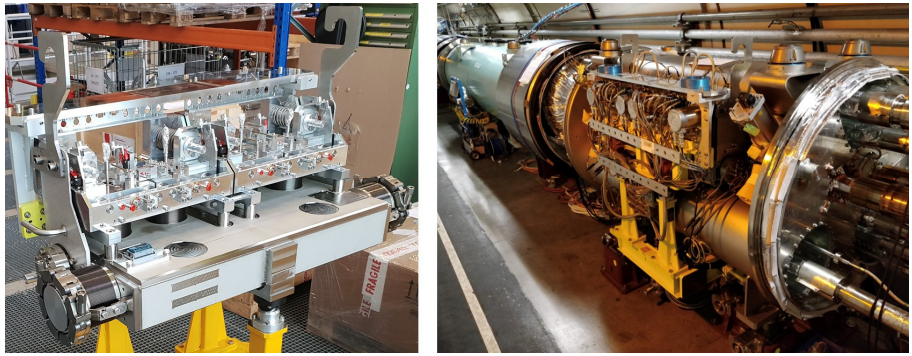

Fig. 5. TCLD collimator for the installation in DSs around IR2 and IR7 (left) and device installed in the connection cryostat in the DS on the left side of IP2 (right). The flange-to-flange distance is 1080 m.

The best performance would be obtained with two TCLD units per beam, however, a single unit gives already a significant performance improvement. It is therefore planned to install one TCLD in IR7 per beam in the HL-LHC baseline, replacing the present main dipole MB.A9 in Cell 9. The old and new IR7 layouts are shown in the left part of Fig. 6.

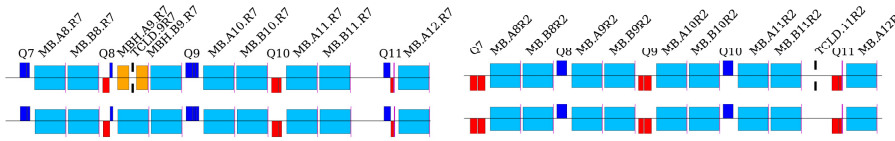

Fig. 6. HL-LHC (top) and LHC (bottom) layouts of the IR7 DS (left) and IR2 DS (right) of B1, with the new TCLD collimators, with and without 11 T dipoles. B2 layouts are symmetric. The beam goes from left to right.

Simulations of this new layout indicate that the power load on the superconducting cables in the main magnets decreases to about 8 mW/cm^3 for protons and 4 mW/cm^3 for Pb ions, thus leaving a comfortable margin to the quench limit. It should be noted that the superconducting cable of the 11 T dipoles instead receives a higher power load of 48 mW/cm^3 with protons (33 mW/cm^3 with Pb ions). However, the quench limit of the new 11 T magnet is estimated to be about 70 mW/cm^3 [36], which is significantly higher than for the present magnets, hence making the losses acceptable, although not with a very large margin. Various mitigation measures to increase this margin are under study, e.g. optimized alignment of the 11 T dipole and a local orbit bump to displace the losses in the 11T magnet to the TCLD. It is thus concluded that the proposed layout with new TCLDs in IR7 mitigates the risk of unacceptably high losses in the DS. These conclusions should be reassessed based on the operational experience in Run 3.

A DS collimation upgrade is needed also for heavy ion collisions in IP2. When two Pb ion beams collide, secondary ion beams with different magnetic rigidity are created, which are lost in the adjacent DS [9,29,37]. These ions represent a source of local heat deposition in the impacted magnet that could lead to a quench. The dominating processes are bound-free pair production (BFPP), where electron–positron pairs are created and one (BFPP1) or two (BFPP2) electrons are caught in a bound state of one of the colliding nuclei, thus changing its charge, and electromagnetic dissociation (EMD), where one nucleus emits one (EMD1) or two (EMD2) neutrons, thus changing mass. Further photon-induced processes also take place, but the four mechanisms mentioned here have the highest cross-sections. An example of ion beams produced in collisions of $^{208}Pb^{82+}$ nuclei in IR2 is given in Fig. 7.

The production of losses above quench limits from these secondary beams was demonstrated experimentally in 2015 at a Pb beam energy of 6.37 Z TeV,

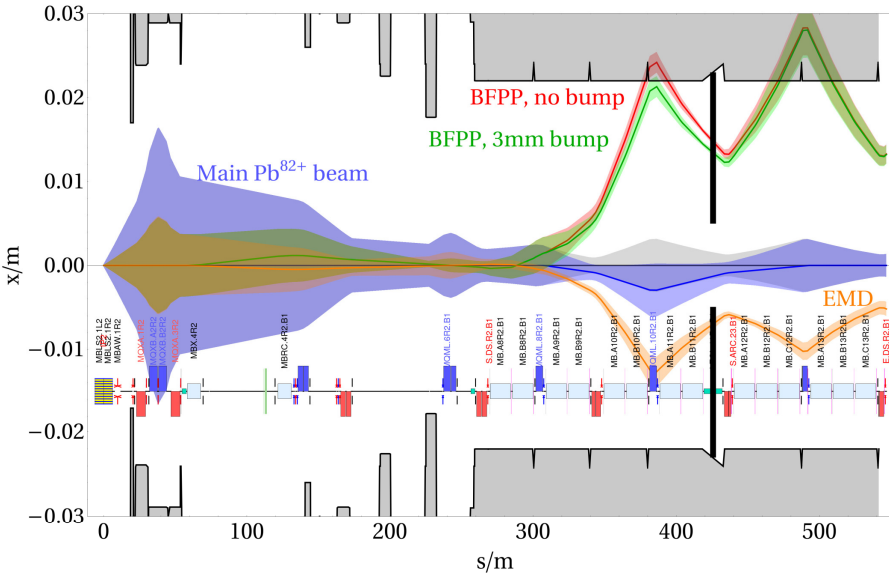

Fig. 7. 1 σ envelope of the main Pb^{82+} beam (violet) together with the dispersive trajectories of ions undergoing BFPP1 (red) and EMD1 (brown), coming out of the ALICE experiment (IP2). The DS collimator jaws appear as black lines. The green line indicates the shifted BFPP1 orbit using a closed orbit bump, which is necessary to intercept the beam with the collimator. The EMD1 beam can be intercepted with the other jaw.

when a dipole quenched at a luminosity of 2.3×10^{27} cm^{-2} s^{-1} [37]. In HL-LHC, with 7 Z TeV energy and a luminosity of about 7×10^{27} cm^{-2} s^{-1} (about seven times the nominal one) [38], the BFPP beam carries 180 W of power. The simulated steady-state load in physics operation on the coils of the MB.B10 dipole is about 50 mW/cm^3 on both sides of the ALICE experiment [38]. Similar ion losses also occur in the DS regions around ATLAS and CMS, however at different locations than in IR2. It is therefore clear that mitigation measures are needed.

In IR1 and IR5, the BFPP1 beam is lost towards the end of the last dipole in Cell 11. This location is close to the connection cryostat. Therefore, the risk of quenches can be mitigated by redirecting the losses on the cryostat beam screen using local orbit bumps. Such bumps have been routinely used in the 2015 [40] and 2018 [41] Pb-Pb runs at 6.37 *Z* TeV. In the latter run, a peak luminosity of 6.2×10^{27} cm^{-2} s^{-1} was reached in IP1 and IP5, which is almost the HL-LHC target luminosity. Simulation studies also confirm

that orbit bumps are a robust solution, indicating that, at a luminosity of 7×10^{27} cm^{-2} s^{-1} and at a beam energy of 7 Z TeV, the power deposition in the coils of downstream magnets and in bus bars would remain safely below the quench level [38].

This solution does not work in IR2, where the BFPP1 beam is instead lost further upstream in Cell 10. It is therefore foreseen to install one TCLD per side in IR2, as shown schematically in Fig. 6. This TCLD intercepts the BFPP1 and EMD1 beams in a location where these ions are well separated from the main beam. The IR2 TCLDs will be installed in the connection cryostat in Cell 11 without need for 11 T dipoles, with the old and new layout shown in the right part of Fig. 6 (right graph). A closed orbit bump is required to make the BFPP1 beam miss the aperture at the first maximum of its trajectory and instead hit the TCLD. The EMD1 beam, which carries ~65 W at a luminosity of 7×10^{27} cm^{-2} s^{-1}, could be intercepted with the other jaw. Similar orbit bumps were successfully deployed operationally in IR1 and IR5 [41].

In order to minimize design and production efforts, the collimator length and material are chosen to be the same as for the TCLDs around IR7. Particle shower simulations with this layout suggest that the power deposition density in the coils of downstream magnets is below 1 mW/cm^3 if the BFPP1 and EMD1 beams impact at least 2 mm from the collimator edges, eliminating the risk of quenching both the magnets and the bus bars in the new connection cryostat [38]. Losses in the DS also occur during proton operation, but simulations have shown that the induced power load is safely below the quench level. Therefore, relying on the orbit bumps to alleviate BFPP losses, no collimation upgrade is needed in the DSs of IR1 and IR5.

5. Upgrades for Impedance Improvement

The LHC impedance budget is largely dominated by the contribution of the LHC collimators [1], which should be reduced to guarantee beam stability (see also Chapter 5). Since this was known already at the LHC design stage, the collimation system has been designed so that every TCS slot in IR3 and IR7 features a companion slot for the future installation of a low-impedance secondary collimator [3], for a total of 22 cabled slots in IR7 and 8 in IR3. Simulations predict that beam stability can be re-established for all HL-LHC scenarios if the carbon-fibre composite (CFC) of present TCSs is replaced, at

least in the betatron cleaning insertion, with a material having an electrical conductivity a factor of 50 to 100 higher than CFC [42]. However, the TCSs should also maintain a high cleaning efficiency, and they could be exposed to large beam losses and must therefore be robust against beam failure.

The latter requirement rules out the possibility to deploy high-Z metals because of their relatively low melting point and comparatively large thermal expansion that impairs their resistance to thermal shocks [43]. The present baseline for the upgraded secondary collimators relies thus on novel carbon-based materials, in particular molybdenum carbide-graphite (MoGr). This is a ceramic composite, jointly developed by CERN and Brevetti Bizz (IT), in which the presence of carbides and carbon fibres strongly catalyses the graphitic ordering of carbon during high temperature processing. This enhances its thermal and electrical properties [42]. To further improve their surface electrical conductivity, these materials will be coated with 5 μm pure molybdenum.

The foreseen HL-LHC upgrade consists therefore of the installation of Mo-coated MoGr collimators in 9 out of 11 TCS slots per beam. The installation is foreseen in two stages: a first installation in the Long Shutdown 2 (LS2, in the period 2019–2021), involving 4 collimators per beam, followed by a second installation in LS3 (2025–2026), when the remaining ones will be installed. This schedule gives already an impedance reduction and operational experience with the new collimators in Run 3, while allowing possible further iterations on the collimator design for the last units. The choice of the slots for installation during LS2 [44] was mainly driven by maximising the impedance reduction for the first upgrade phase, while avoiding installation slots with the highest expected thermo-mechanical loads, as an extra safety measure for validating the design.

The HL-LHC impedance upgrade includes a contribution to low-impedance material also for the TCPs that are otherwise renewed as a part of the consolidation project. In LS2, the 4 IR7 TCPs in the horizontal and vertical planes in both beams will be replaced with the new design using uncoated MoGr and introducing the BPM functionality [19]. Since TCPs are continuously exposed to primary beam losses, coating the active jaw part is not considered viable. The MoGr provides an improvement of about a factor 5 in resistivity compared to CFC, while ensuring a similar robustness against beam failure.

The impedance of the present and future machine configurations was studied through detailed calculations. Fig. 8 shows the expected octupole current required to stabilise the HL-LHC beam for the ultimate scenario [44] (see also [45] and Chapter 5 of this book), i.e. the most demanding one from the point of view of beam stability, together with the maximum allowed octupole current of 570 A. Estimations are done taking into account all sources of machine impedance, including crab-cavities, and a factor 2 as it was observed at the end of Run 2, also after optimization of coupling that was confirmed to be a major detrimental mechanism for beam stability [46]. As seen, beam stability requires an impedance upgrade. Moreover, the estimation for the present upgrade almost matches the maximum octupole current, with an almost negligible deterioration due to the two TCS slots not upgraded. Expectations for the LS2 upgrade show a significant improvement already achieved with only four collimators per beam (where also the TCP is upgraded through the consolidation program to uncoated MoGr). This discrepancy is

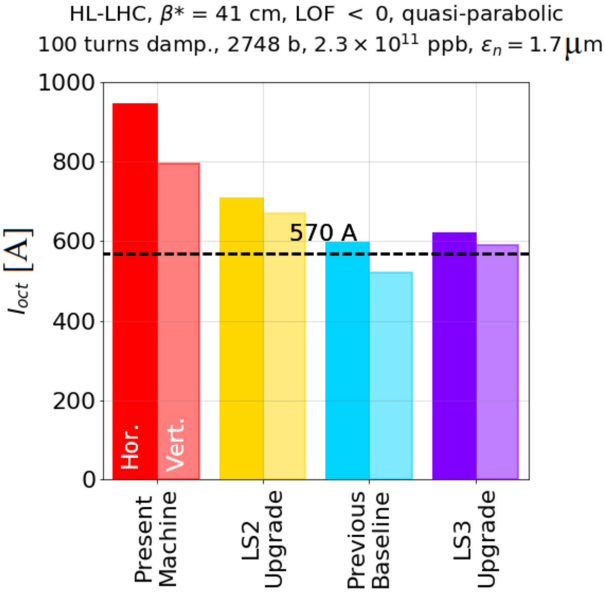

Fig. 8. Expected octupole current required to stabilise the HL-LHC beam for the ultimate scenario [44]. with the relevant simulation parameters. Expectation values include the factor 2 discrepancy between predictions and operational values observed in Run 2 (after optimisation of the parameters such as linear coupling).

being investigated in detail and seems to be related to noise injected in the beam by power supplies or by the transverse damper [47].

The thermo–mechanical response of the new collimator has been simulated to ensure that it will survive regular and accidental beam losses [24]. Simulations are done in three steps, including particle tracking, energy deposition, and thermo-mechanical analysis. The studies demonstrate that the most loaded low-impedance collimator, which intercepts about 100 kW during a 0.2 h beam lifetime, survives without permanent damage but is subject to a jaw deformation of 500 μm, exceeding the tolerance of 100 μm. However, the deformation is directed away from the beam, meaning that the expected impact on the cleaning efficiency is very small. Nevertheless, this particular TCS will be upgraded only in LS3, giving time to further improve the design if needed based on the operational experience of Run 3.

The new collimator design must be validated for operation in the LHC. For this purpose, a rich programme of validation tests has been carried out. Irradiation tests of MoGr at GSI and BNL are well advanced, and the latest results indicate that MoGr, even when coated with Mo, can survive the expected dose in HL-LHC, although the analysis is not yet finalized at the time of writing (see for example [48] for the un-coated case). Experimental beam-impact tests at HiRadMat were carried out very successfully to demonstrate that a full-scale MoGr jaw prototype could be hit by a full train during an injection failure without apparent damage [24]. The coating was assessed in another HiRadMat test [49], where an 8 μm-thick Mo coating layer exhibited a surface scratch less than 2 mm wide following a direct impact equivalent to the HL-LHC injection failure. Such a damage is non-catastrophic from the impedance point of view; moreover, thanks to the limited transverse extension of the damage, an undamaged portion of jaw surface can be exposed to the beam by moving the collimator in the non-collimation plane thanks to the so-called 5^{th} axis functionality.

Tests of a prototype collimator with circulating beams in the LHC have been carried out in 2017. Each jaw of the prototype was built with MoGr bulk and has three different surface "stripes" for impedance tests: uncoated MoGr, Mo coating and TiN coating. The collimator was installed right next to the CFC TCS with the smallest beam size in the collimation plane, hence maximizing the effect on impedance. Both collimators are vertical, allowing for a direct comparison. Fig. 9 shows the tune-shift measurements with the

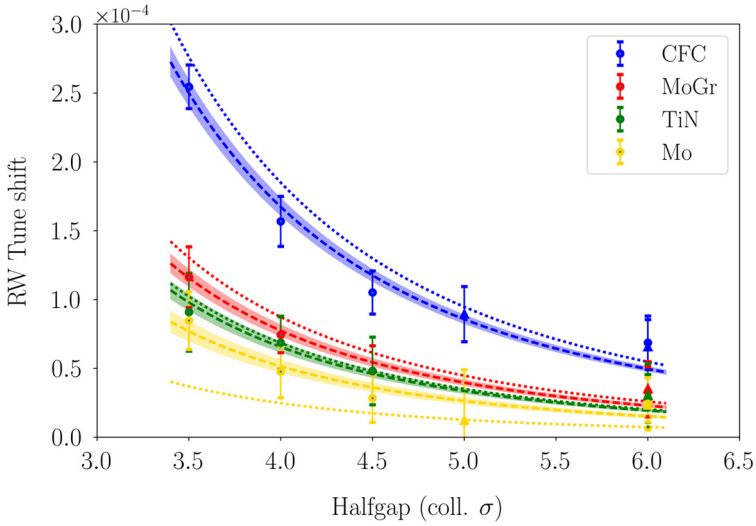

Fig. 9. Tune shift measurements carried out in 2017 (dots), fit to experimental data (dashed line) and predictions (dotted lines) for the three stripes of the TCSPM prototype and the CFC of regular TCSGs as a function of the minimum collimator opening [44]. The collimator opening is expressed as half gap, in units of local beam σ (for a normalised emittance of 3.5 μm).

MoGr prototype and the adjacent CFC TCS, taken while varying the collimator opening [45]. The measurements are compared to numerical simulation results. In general, a good agreement is seen between simulations and measurements, with the exception of the Mo coating, which shows a factor 2 discrepancy. Further measurements in laboratory showed that the quality of the microstructure of the coating and of the jaw roughness could explain this difference [50]. The MoGr prototype was kept in the LHC throughout 2018 and used throughout the run at the same settings as the adjacent TCS, without any fault or odd behavior in key operational parameters and observables.

6. Reference Cleaning Performance for the Baseline Upgrade System

Putting together all upgrades described in the previous sections, the global performance of the upgraded HL-LHC collimation system should be assessed. This has been done using the SixTrack-FLUKA coupling [27], which tracks an initial distribution of beam halo particles through the magnetic lattice of

the ring. When a particle enters a collimator, its coordinates are sent to FLUKA, which simulates the particle-matter interaction and then sends any surviving particles above a minimum threshold back to SixTrack for further tracking. A particle is considered lost either when it hits the aperture (the particle coordinates are checked against a detailed aperture model with 10 cm longitudinal precision) or if it interacts inelastically inside a collimator. The exception to this is single diffractive events, where the incident proton could survive and exit the collimator. These protons, which often have significant energy offsets, are tracked further. The simulation output contains coordinates of all loss locations.

The simulation output, presented as a loss distribution around the ring, is shown in Fig. 10 for the reference case of horizontal betatron losses at 7 TeV for Beam 1. The baseline collision optics with β^*=15 cm, version 1.3, was used together with the collimator settings in Table 1. As can be seen, the main losses occur at the betatron collimators in IR7 and losses at other positions in the ring are orders of magnitude lower. The most important losses outside of IR7 occur at the momentum collimators in IR3 and at the dump protection collimators in IR6, while significant losses occur also at the TCTs at the experiments. It should be noted that almost no cold losses occur outside of IR7, which is an excellent result, possible only thanks to the very efficient cleaning of the TCLD. The highest cold losses in the ring occur at the first 11 T magnet, just upstream of the TCLD as discussed in Section 4. The resulting energy deposition here is below the estimated quench limit even for the pessimistic case of a 0.2 h beam lifetime, meaning that the collimation system successfully protects the cold elements. These results are qualitatively representative also for vertical losses (similar loss pattern) and for losses in B2 (similar loss pattern, but with the beam going in the opposite direction). Off-momentum losses in IR3 are not expected to limit the performance of HL-LHC [51].

Similar cleaning simulations have been performed also for Pb ion beams. As observed in the LHC machine [51,53], the nuclear fragmentation makes the collimation system less efficient with ion beams than with protons, however, this is to a large part compensated by the lower stored beam energy. The TCLD cleans almost completely the particles that would otherwise be lost around the ring, and the only significant cold losses are in the IR7 DS, on the 11 T magnet upstream of the TCLD. The energy deposition studies in Section 4 show that these losses are well below the quench level.

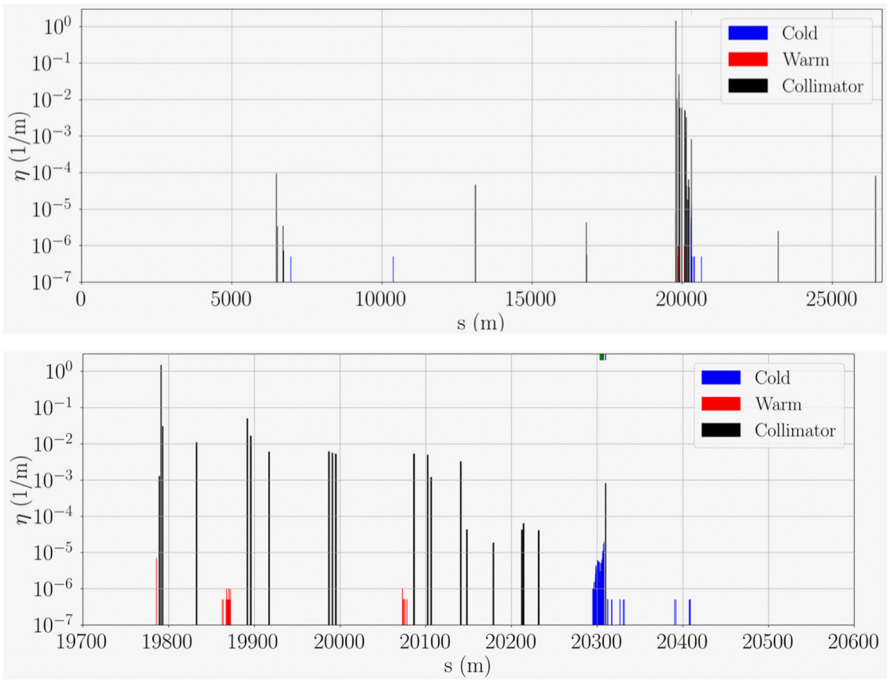

Fig. 10. The simulated losses around the HL-LHC ring (top) with a zoom in the betatron cleaning in IR7 (bottom). The losses, simulated for horizontal betatron losses in lattice version HL-LHC v1.3 at β*=15 cm, are expressed in terms of local cleaning efficiency as in [3]. Courtesy of E. Belli.

7. Enhanced Beam Collimation with Hollow Electron Beams

In this section we discuss a new, more advanced, collimation concept that has been very recently (2019) integrated into the upgrade baseline following the Cost & Schedule Review in 2019 through a substantial in-kind contribution (under signature at the time of writing). The concept of hollow electron lenses (HELs) collimation is presented. These two items, which are schematically illustrated in Fig. 11, are part of the approved studies within WP5. Focus was put in recent years to review the needs for these upgrades for HL-LHC and to demonstrate the required technology in tests without and with beam. Both crystal collimation and HELs address, in different ways, further improvements of the betatron collimation system (crystal collimation will be discussed in Chapter 30).

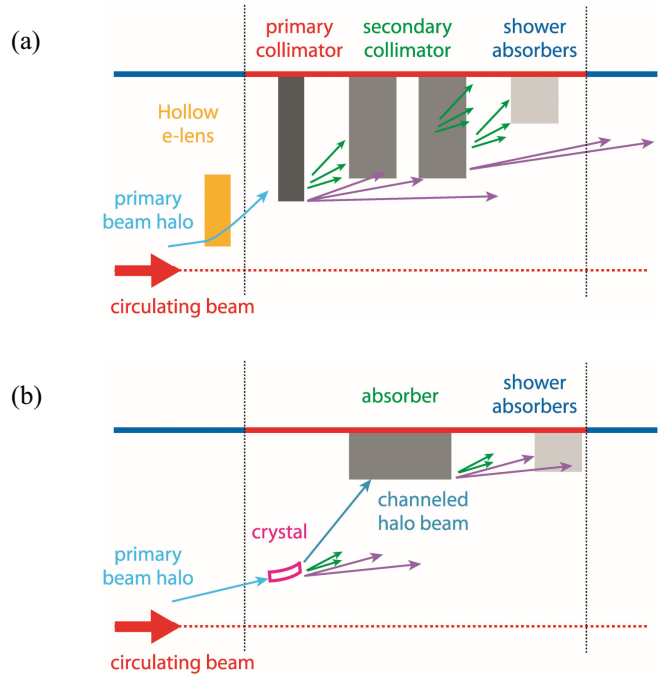

Fig. 11. Illustrative view of the b betatron collimation system (a) with integrated hollow e-lens or equivalent halo diffusion mechanism; (b) with an ideal crystal-based collimation system. Halo control techniques are used to change the diffusion speed of halo particles, and rely on the full collimation system remaining in place for their disposal. The crystal-based scheme entails a change of concept for betatron collimation, where the whole beam losses are concentrated, ideally, in one single beam absorber per plane.

Operational experience in 2012 indicated that the LHC collimation would profit from halo control mechanisms. The operation of Run 2 at 6.5 TeV showed a less severe impact from halo losses [54]; however, scaling them to HL-LHC beam parameters is still a source of concerns. In particular, the presence of over-populated tails in the LHC beams was consistently observed in dedicated measurements at the LHC [55,56]. Simple extrapolations to the HL-LHC beam intensities lead to the estimate that more than 30 MJ can be stored at transverse amplitudes between 3.5-4.0 σ and the aperture of primary collimators. This scenario, in particular considering that crab-cavities might produce new fast-loss failure scenarios at HL-LHC, requires an active control of tails. The HELs are the most promising solution to achieve this goal.

Halo control mechanisms were used in other machines like HERA and the Tevatron [57], and more recently in the RHIC [58]. The idea is that, by controlling the diffusion speed of halo particles, one can (1) act on the time profile of the losses, for example by reducing rates of losses that would otherwise take place in a short time, and (2) control the population of halo particles in a certain range of transverse apertures.

In a HEL, a hollow electron beam runs parallel and concentrically to the proton or ion beam. The hollow beam produces an electromagnetic field only affecting halo particles above a given transverse amplitude determined by its inner radius, changing their transverse diffusion speed. Such a device is integrated into the existing collimation system – which remains responsible for the safe and efficient disposal of halo particles – as follows: the electron beam's inner radius is smaller than the TCP aperture, producing a region of depleted halo between the beam core and the primary collimator aperture. A solid experimental basis achieved at the Tevatron indicates that this solution is promising and can be applied to the LHC as well [57 and references therein].

The potential advantages of electron lens collimation are multiple.

- Control loss rates on primary collimators, with potential mitigation of peak loss rates in cold magnets.
- Mitigate risk of damage from beam losses in case of fast failures with tens of MJ in the tails.
- Reduce tail populations and peak loss rates in the case of orbit drifts.
- Tighten the collimator hierarchy for a smaller β^* reach, thanks to reduced tails (compatibly with other constraints like impedance budget).
- Scraping the beam at very low amplitudes ($>3\,\sigma$) without the risk of damage, as expected for bulk scrapers.
- Tune the impact parameters on the primary collimators with a possible improvement in cleaning efficiency.

The HEL for the HL-LHC [59] is targeted at enabling active control of beam tails above 3 to 4 real beam sigmas, with tail depletion efficiencies of the order of 90% over times of tens of seconds. This should be possible, ideally, in all phases of the operational cycle but specifically at top energy when beam losses are a concern (usage at injection is considered as an asset for the initial commissioning phase). The present design parameters of the HL-LHC lenses, optimized for 7 TeV, are given in Table 2 and a 3D drawing is given in

Fig. 12. Note that the HEL design should ensure: (i) the possibility of pulsing the current turn-by-turn (as required to drive resonances in the halo particle's dynamics); (ii) a train-by-train selective excitation (leaving 'witness' trains with populated halos for diagnostics and machine protection purposes).

The main HEL components are (1) the electron beam generation and disposal systems: electron gun and collector; (2) the superconducting magnet system composed by main 5 T solenoids, solenoids at the e-beam generation and correctors to stabilize and steer the electron beam; (3) beam instrumentation for the optimization of the electron beam: beam position and transverse profile monitors (see Chapter 18). The LHC Point 4 that houses the superconducting RF system is considered for installation of the HEL, and suitable

Table 2. Hollow electron beam equipment parameters.

Parameter	Value or range
Geometry	
Length of the interaction region, L [m]	3
Desired transverse scraping range at 7 TeV [σ, $\epsilon = 2.5\mu$m]	3.6-7.5
Range of inner electron beam radii at 7 TeV [mm]	1.1-2.3
Inner vacuum chamber diameter [mm]	60
Magnetic fields at 7 TeV and magnet parameters	
Main solenoid field, B_m [T]	5.0
Range of gun solenoid field, B_g [T]	0.2-4.0
Nominl gun solenoidnfield, B_g [T]	0.375
Range of compression factors, $\sqrt{B_m/B_g}$	1.1-5.0
Target compression factor, $\sqrt{B_m/B_g}$	3.7
Electron gun and high-voltage modulator	
Inner/outer cathode diameters [mm]	8.05-16.1
Peak yield at 10 kV, I [A]	5
Cathode-anode voltage [kV]	10
Accelerating voltage [kV]	15
Rise time (10%-90%) [ns]	200
Electron pulse duration for pulsed operation [μs]	1.2-86.0
Repetition rate [kHz]	11.4-34.2

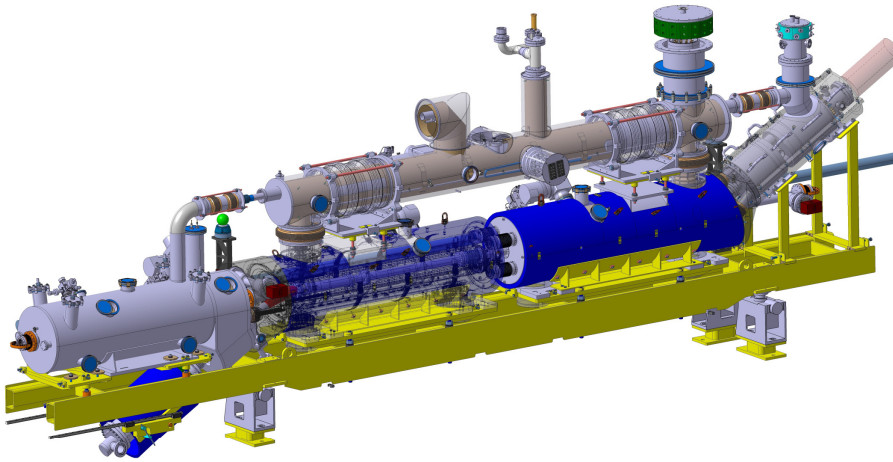

Fig. 12. Present design of the HL-LHC hollow e-lens (version Nov. 2020). An 'S' shape is proposed in order to self-compensate potential kicks from the e-beams asymmetries seen by the proton beam at entry and exit. Courtesy of D. Perini.

locations have been identified for the integration of two HELs, one per beam. The HEL does not generate significant local beam losses as the particles slowly expelled from the tails are disposed of in IR7 through the standard multi-turn cleaning mechanism.

References

1. I. Béjar Alonso et al., High-Luminosity Larger Hadron Collider (HL-LHC): Technical Design Report, CERN Yellow Reports: Monographs, 10/2020.
2. O. Brüning (Ed.) et al., LHC Design Report Vol. 1, CERN-2004-003-V-1 (2004).
3. R. Assmann et al., The final collimation system for the LHC, Proc. EPAC2006, Edinburgh, 2006. Conf. Proc. C060626 (2006) 986-988. Also as CERN-LHC-PROJECT-REPORT-919 (2006).
4. S. Redaelli et al., Chapter 5: Collimation system, CERN Yellow Rep. Monogr. 10 (2020) 87-114.
5. S. Redaelli, Beam Cleaning and Collimation Systems, CERN Yellow Report CERN-2016-002, pp.403-437. Contribution to: 2014 Joint International Accelerator School.
6. R. Bruce, R.W. Assmann and S. Redaelli, Calculations of safe collimator settings and β^* at the Large Hadron Collider, Phys. Rev. ST Accel. Beams 18, 061001 (2015).
7. R. Bruce et al., Reaching record-low β* at the CERN Large Hadron Collider using a novel scheme of collimator settings and optics, Nucl. Instrum. Methods Phys. Res. A 848 (2017).

8. D. Mirarchi et al., Cleaning Performance of the Collimation System of the High Luminosity Large Hadron Collider, Proceedings, 7th International Particle Accelerator Conference (IPAC 2016): Busan, Korea, May 8-13, 2016, doi 10.18429/JACoW-IPAC2016-WEPMW007.
9. R. Bruce et al., Observations of Beam Losses Due to Bound-Free Pair Production in a Heavy-Ion Collider, Phys. Rev. Letters 99.14 (2007).
10. R. Bruce et al., Sources of machine-induced background in the ATLAS and CMS detectors at the CERN Large Hadron Collider, Nucl. Instrum. Methods Phys. Res. A 729 (2013) 825–840.
11. R. Bruce et al., Collimation-induced experimental background studies at the CERN Large Hadron Collider, Phys. Rev. Accel. Beams 22, 021004 (2019).
12. E. Quaranta et al., Modeling of beam-induced damage of the LHC tertiary collimators, Phys. Rev. Accel. Beams 20 (2017) no.9, 091002.
13. B. Salvachua Ferrando et al., Cleaning performance of the LHC Collimation System up to 4 TeV, Proc. IPAC13, Shanghai, China, 2013. http://accelconf.web.cern.ch/accelconf/ipac2013/papers/mopwo048.pdf.
14. N. Fuster Martinez et al., Run 2 Collimation Overview, Proceedings of the 2019 Evian Workshop on LHC Beam Operations, pp. 149-164, https://cds.cern.ch/record/2750291?ln=fr.
15. Z. Citron et al., Future physics opportunities for high-density QCD at the LHC with heavy-ion and proton beams, CERN-LPCC-2018-07 (2018).
16. S. Redaelli et al., Final implementation and performance of the LHC collimator control system, Proc. PAC09, Vancouver (CA). Conference: C09-05-04, FR5REP007.
17. F. Carra et al., Mechanical engineering and design of novel collimators for HL-LHC, Proc. IPAC2014, Dresden, Germany, 2014. http://accelconf.web.cern.ch/IPAC2014/papers/mopro116.pdf.
18. A. Bertarelli et al., The mechanical design for the LHC Collimators, Proc. EPAC2004, Lucerne, Switzerland, 2004. https://accelconf.web.cern.ch/e04/PAPERS/MOPLT008.PDF.
19. A. Dallocchio et al., LHC collimators with embedded beam position monitors: A new advanced mechanical design, Proc. IPAC2011, San Sebastian, Spain, IPAC-2011-TUPS035 (2011).
20. G. Valentino et al., Successive approximation algorithm for BPM-based LHC collimator alignment, Phys. Rev. ST Accel. Beams 17, 021005 (2014).
21. G. Valentino et al., Final implementation, commissioning, and performance of embedded collimator beam position monitors in the Large Hadron Collider, Phys. Rev. Accel. Beams 20, 081002 (2017).
22. D. Wollmann et al., Beam feasibility study of a collimator with in-jaw beam position monitors, Nucl. Instrum. Methods Phys. Res., Sect. A 768, 62 (2014).
23. A. Bertarelli et al., An experiment to test advanced materials impacted by intense proton pulses at CERN HiRadMat facility, Nucl. Instr. Meth. B 308 (2013) 88.

24. G. Gobbi et al., Novel LHC collimator materials: High-energy Hadron beam impact tests and nondestructive post irradiation examination, Mechanics of Advanced Materials and Structures 1-13, DOI: 10.1080/15376494.2018.1518501 (2019).
25. F. Carra et al., Mechanical robustness of HL-LHC collimator designs, J. Phys.: Conf. Ser. 1350 012083 (2019).
26. A. Bertarelli et al., Dynamic testing and characterization of advanced materials in a new experiment at CERN HiRadMat facility, J. Phys.: Conf. Ser. 1067 082021 (2018).
27. S. Redaelli (Ed.), Proceedings of ICFA Mini-Workshop on Tracking for Collimation in Particle Accelerators. CERN-2018-011-CP (2018).
28. R. Bruce et al., Simulations and measurements of beam loss patterns at the CERN Large Hadron Collider, Phys. Rev. ST Accel. Beams 17 (2014), p.081004. doi: 10.1103/PhysRevSTAB.17.081004.
29. R. Bruce et al., Beam losses from ultraperipheral nuclear collisions between 208Pb82+ ions in the Large Hadron Collider and their alleviation, Phys. Rev. ST Accel. Beams 12 (2009) 071002.
30. B. Auchmann et al., Testing Beam-Induced Quench Levels of LHC Superconducting Magnets, Phys. Rev. ST Accel. Beams 18 (2015) 061002.
31. P. D. Hermes et al., LHC Heavy-Ion Collimation Quench Test at 6.37Z TeV, CERN-ACC-Note-2016-0031 (2016).
32. P. D. Hermes, Heavy-ion collimation at the Large Hadron Collider - Simulations and measurements, Ph.D. thesis, University of Munster, DE (2016). CERN-THESIS-2016-230.
33. A. Ferrari, P.R. Sala, A. Fassò, and J. Ranft, FLUKA: a multi-particle transport code, CERN 2005-10 (2005), INFN/TC_05/11, SLAC-R-773.
34. A. Lechner et al., Validation of energy deposition simulations for proton and heavy ion losses in the CERN Large Hadron Collider, Phys. Rev. Accel. Beams 22 (2019) 7, 071003.
35. E. Skordis et al., Study of the 2015 Top Energy LHC Collimation Quench Tests Through an Advanced Simulation Chain, doi:10.18429/JACoW-IPAC2017-MOPAB012.
36. L. Bottura et al., Quench performance and assumptions: magnets and cryogenics, presentation at the International Review of the HL-LHC Collimation System (2019). INDICO: 780182.
37. M. Schaumann et al., Bound-free pair production from nuclear collisions and the steady-state quench limit of the main dipole magnets of the CERN Large Hadron Collider, Phys. Rev. Accel. Beams 23 (2020) 121003.
38. R. Bruce et al., Performance and luminosity models for heavy-ion operation at the CERN Large Hadron Collider, Eur. Phys. J. Plus 136, 745 (2021). https://doi.org/10.1140/epjp/s13360-021-01685-5.
39. C. Bahamonde Castro et al., Power deposition in LHC magnets due to bound-free pair production in the experimental insertions, Proceedings of IPAC2016, Busan, Korea, TUPMW006, pp. 1418-1421.
40. J.M. Jowett et al., The 2015 heavy-ion run of the LHC, Proceedings of IPAC16, Busan, Korea, TUPMW027, pp. 1493-1496. DOI: 10.18429/JACoW-IPAC2016-TUPMW027.

41. J.M. Jowett et al., Overview of ion runs during run 2, Proc. 9th LHC Operations Evian Workshop, Evian, France (2019).
42. J. Guardia-Valenzuela et al., Development and properties of high thermal conductivity molybdenum carbide - graphite composites, Carbon 135 (2018) 72-84.
43. A. Bertarelli, Beam Induced Damage Mechanisms and Their Calculation, CERN Yellow Report CERN-2016-002, pp. 159-227. Contribution to: 2014 Joint International Accelerator School.
44. S. Antipov et al., Staged implementation of low-impedance collimation in IR7: plans for LS2, CERN-ACC-2019-0001, CERN, Geneva, Switzerland (2019). https://cds.cern.ch/record/2654779/files/CERN-ACC-NOTE-2019-0001.pdf.
45. S. Antipov et al., Transverse beam stability with low-impedance collimators in the High-Luminosity Large Hadron Collider: Status and challenges, Phys. Rev. Accel. Beams 23 (2020) 3, 034403, https://inspirehep.net/literature/1760250.
46. L.R. Carver et al., Transverse beam instabilities in the presence of linear coupling in the Large Hadron Collider, Phys. Rev. Accel. Beams 21 (2018) 4, 044401.
47. S.V. Furuseth et al., Loss of transverse Landau damping by noise and wakefield driven diffusion, Phys. Rev. Accel. Beams 23 (2020) 11, 114401.
48. N. Simos et al., Proton irradiation effects in Molybdenum-Carbide-Graphite composites, J. Nucl. Mater. 553 (2021) 153049.
49. M. Pasquali et al., Dynamic Response of Advanced Materials Impacted by Particle Beams: The MultiMat Experiment, Journal of Dynamic Behavior of Materials 5 (2019) 3, 266-295.
50. N. Biancacci et al., Resistivity Characterization of Molybdenum-Coated Graphite-Based Substrates for High-Luminosity LHC Collimators, Coatings 2020, 10(4), 361; https://doi.org/10.3390/coatings10040361.
51. H. Garcia Morales et al., Off-momentum cleaning simulations and measurements at the Large Hadron Collider, Nuclear Instruments and Methods in Physics Research Section A: Accelerators, Spectrometers, Detectors and Associated Equipment 1010 (2021), p. 165494. doi: https://doi.org/10.1016/j.nima.2021.165494.
52. P.D. Hermes et al., Measured and simulated heavy-ion beam loss patterns at the CERN Large Hadron Collider, Nucl. Instrum. Meth. A 819 (2016) 73-83.
53. N. Fuster-Martínez et al., Simulations of heavy-ion halo collimation at the CERN Large Hadron Collider: Benchmark with measurements and cleaning performance evaluation, Phys. Rev. Accel. Beams 23 (2020) 11, 111002.
54. Review of the needs for a hollow e-lens for the HL-LHC, 6th – 7th October 2016, CERN, Geneva, Switzerland. https://indico.cern.ch/event/567839.
55. G. Valentino et al., Beam diffusion measurements using collimator scans at the LHC, Phys. Rev. Spec. Top. Accel. Beams 16 (2013) 021003.
56. A. Gorzawski et al., Probing LHC halo dynamics using collimator loss rates at 6.5 TeV, Phys. Rev. Accel. Beams 23 (2020) 4, 044802.
57. G. Stancari, A. Valishev, G. Annala, G. Kuznetsov, V. Shiltsev, D.A. Still et al., Collimation with hollow electron beams, Phys. Rev. Lett. 107 (2011) 084802 [arXiv:1105.3256].

58. X. Gu et al., Halo removal experiments with hollow electron lens in the BNL Relativistic Heavy Ion Collider, Phys. Rev. Accel. Beams 23 (2020) 3, 031001.
59. S. Redaelli et al., Hollow electron lenses for beam collimation at the High-Luminosity Large Hadron Collider (HL-LHC), JINST 16 (2021) 03, P03042.